Original Article

Multimodal imaging for the differential diagnosis and efficacy evaluation of intraocular retinoblastoma in children with selective ophthalmic artery infusion

Jianshe Zhao[1,2], Ruodi Cui[2], Lin Li[2], Bing Zhao[2], Long Chen[1]

[1]Department of Interventional Radiology, The First Affiliated Hospital of Soochow University, Suzhou, China; [2]Center of Medical Imaging, Children's Hospital Affiliated Shandong University, Jinan Children's Hospital, Jinan, China

Contributions: (I) Conception and design: J Zhao, L Chen; (II) Administrative support: J Zhao, L Chen; (III) Provision of study materials or patients: J Zhao, R Cui, L Li, B Zhao; (IV) Collection and assembly of data: J Zhao, L Li, B Zhao; (V) Data analysis and interpretation: J Zhao, R Cui, L Li, B Zhao; (VI) Manuscript writing: All authors; (VII) Final approval of manuscript: All authors.

Correspondence to: Prof. Long Chen, PhD. Department of Interventional Radiology, The First Affiliated Hospital of Soochow University, 899 Pinghai Road, Gusu District, Suzhou 215006, China. Email: chenlongir@163.com.

Background: Retinoblastoma (RB) is the most common malignant tumor in children under the age of 3 years and is associated with a high disability and mortality rate. The aim of this study was, first, to evaluate the clinical efficacy of multimodal imaging in differentially diagnosing RB in children and in predicting the efficacy of selective ophthalmic artery infusion (SOAI) and, second, to identify the factors associated with this efficacy.

Methods: This study retrospectively collected the data from 256 children with unilateral RB and intraocular involvement, including multimodal imaging magnetic resonance imaging (MRI), computed tomography (CT), and clinical characteristics. Among the cases, 33 with both CT and MRI data available were used to evaluate the diagnostic accuracy in distinguishing RB, with histopathological results serving as the gold standard. Additionally, a retrospective analysis was conducted on the MRI and clinical characteristics of 256 cases of unilateral RB with intraocular involvement before SOAI treatment. The predictive ability of imaging features and clinical characteristics for the treatment efficacy of children was analyzed, and the differences in globe salvage rates and visual preservation based on different tumor stages were evaluated.

Results: The diagnostic accuracy of CT imaging for RB was 96.96% while that of MRI was 84.84%, with both showing high consistency with the histopathological results. CT images demonstrated a posterior intraocular mass with a high-density appearance, with spots, patches, or clustered calcifications visible within the tumor. The CT values were mostly above 100 Hounsfield units (HU), and enhanced scanning showed varying degrees of enhancement in noncalcified masses. MRI showed low or moderate signal intensity on T1-weighted images and moderate-to-high signal intensity on T2-weighted images, with significant enhancement after contrast administration. Tumors with more calcifications showed long T1 and short T2 signals. Patients with better prognosis had a higher delta signal increase (ΔSI), a greater distance from the optic disc, smaller tumor diameter, absence of implantation nodules or smaller implantation range, endogenous growth pattern, smaller extent of retinal detachment, absence of clinical high-risk factors, no vitreous hemorrhage, no globe shrinkage, and smaller calcification volume. The distance between the tumor and optic disc, clinical high-risk factors, and tumor growth pattern were found to be independent factors associated with prognosis. The rate of successful globe salvage and visual acuity decreased with increasing tumor stage.

Conclusions: CT and MRI are highly valuable for the comprehensive assessment of tumors in pediatric RB. MRI alone can complete a comprehensive assessment of patients with RB and thus allow for the reduction radiation dose in children. Calcification of the tumor is crucial for diagnosis, and imaging findings can serve to inform patient prognosis and treatment planning. The distance between the tumor and optic disc, clinical high-risk factors, and tumor growth pattern are closely related to the prognosis of children.

Keywords: Differential diagnosis; multimodal imaging; child; retinoblastoma (RB)

Submitted Jan 04, 2024. Accepted for publication May 31, 2024. Published online Jul 11, 2024.
doi: 10.21037/tp-24-2
View this article at: https://dx.doi.org/10.21037/tp-24-2

Introduction

Retinoblastoma (RB) is one of the most common malignant tumors in children under the age of 3 years and has a high disability and mortality rate (1), with a death rate of 40% to 70% in developing countries, posing a significant threat to the lives of affected children (2). RB originates from the granular layer cells within the retina, with nonhereditary cases accounting for 40% of cases and no racial or gender differences being observed (3). RB predominantly affects one eye and is caused by genetic alterations that disrupt the normal cell division regulation in retinal cells (4).

The classification of RB based on its severity is an essential basis for determining treatment plans and assessing prognosis. In 1968, the American Joint Committee on Cancer (AJCC) introduced the tumor-node-metastasis (TNM) staging system for solid malignant tumors, which can be used to evaluate the overall prognosis of RB. The internationally recognized classification system for intraocular RB, known as the International Intraocular Retinoblastoma Classification (IIRC), currently plays a significant role in assessing prognosis and guiding the selection of systemic chemotherapy and focal treatment methods. However, it is important to note that IIRC is specifically designed for intraocular RB. There are two different versions of the IIRC: the Los Angeles version proposed by Linn Murphree *et al.* in 2005 (5) and the Philadelphia version released by Shields *et al.* in 2006 (6). The primary difference between these two staging methods lies in the varying definitions of intraocular tumor stages C, D, and E (7). Given the influence of various factors such as extraocular tumor growth and calcification on staging, the use of imaging diagnosis is not only necessary but also highly accurate.

In clinical practice, leukocoria is a typical manifestation of RB, characterized by the presence of a gray or yellowish spherical masses in the fundus of the eye. Other symptoms may include glaucoma, an enlarged eyeball, and protrusion (8,9). RB tumors tend to progress rapidly, leading to systemic metastasis and poor prognosis. Early diagnosis is challenging, resulting in a relatively high rate of misdiagnosis and missed diagnosis. Imaging techniques, especially computed tomography (CT) and magnetic resonance imaging (MRI), play a critical role in the differential diagnosis of RB, aiding in accurate classification, staging, and treatment planning for affected children. Reports suggest that early diagnosis and selection of the appropriate treatment approach are crucial for improving the prognosis of those with RB and minimizing visual impairment (10).

The treatment principles for pediatric RB aim to preserve the eye and visual function while ensuring survival. Selective ophthalmic artery infusion (SOAI) has emerged as a promising alternative for the treatment of RB (11), potentially replacing systemic chemotherapy or external beam radiation therapy. With SOAI, chemotherapy drugs are selectively delivered via the ophthalmic artery, allowing for targeted delivery to the tumor while minimizing systemic side effects (12). This local treatment modality has shown good tumor control and preservation of visual function.

Highlight box

Key findings

- Magnetic resonance imaging (MRI) is crucial for diagnosing and evaluating pediatric retinoblastoma (RB).
- The presence of calcification, along with factors including distance from the optic disc, clinical high-risk factors, and tumor growth pattern are significantly associated with prognosis.
- As tumor stage increases, the rate of successful globe salvage and visual acuity decreases.

What is known and what is new?

- This study supports the importance and usefulness computed tomography and MRI in diagnosing and evaluating RB in pediatric patients, emphasizes the critical role of calcification in tumor diagnosis, and identifies significant prognostic factors.
- MRI alone is sufficient for comprehensively assessing RB, and the integration of calcification and factors such as tumor location, high-risk factors, and growth pattern can aid in the prognosis and the customization of treatment.

What is the implication, and what should change now?

- Radiologists and ophthalmologists should collaborate in the accurate diagnosis and evaluation of RB in children.

Despite its effectiveness being well-established (13), a portion of patients still experience suboptimal prognosis, which can lead to enucleation or death (14). Therefore, comprehensive imaging evaluation is crucial for predicting the prognosis of SOAI treatment. To this end, the accurate assessment of tumor parameters before treatment and selection of appropriate diagnostic and therapeutic approaches are of paramount importance for prognosis. Multimodal MRI, with its high soft tissue resolution and multiple imaging sequences (15), has become the preferred imaging modality for assessing those with RB.

This study aimed to analyze the radiological manifestations of RB in CT and MRI, compare their diagnostic accuracy, and further analyze the multimodal MRI scans of patients with unilateral RB across different stages. By comparing the differences in tumor-disc distance, clinical high-risk factors, foci, growth patterns, tumor volume, and retinal detachment between patients with successful eye preservation and those with failure, we aimed to identify independent predictive factors associated with prognosis of patients with RB. This study can provide solid and reliable evidence for selecting optimal clinical diagnostic and treatment plans. We present this article in accordance with the STROBE reporting checklist (available at https://tp.amegroups.com/article/view/10.21037/tp-24-2/rc).

Methods

Patients

The patients with RB included in this study were recruited from Shandong University Affiliated Children's Hospital from June 2016 to August 2020. The inclusion criteria were as follows: (I) RB with unilateral involvement in stages B to E according to IIRC criteria (6); (II) an initial treatment of comprehensive therapy with SOAI; and (III) successful eye-preserving treatment with a follow-up period of 2 to 5 years, starting from the first follow-up visit 3 months after completion of comprehensive chemotherapy for the patient. The examinations included funduscopy and MRI (with CT images used for comparison and discrimination efficacy in some patients). Stable disease without recurrence and the presence of varying degrees of calcification, scar formation, and fish flesh-like changes in the original tumor area as determined by fundus examination were the final inclusion criteria. Meanwhile, the exclusion criteria were as follows: (I) noncompliance with treatment or failure to attend scheduled follow-up visits after discharge and (II) missing MRI data and poor image quality that did not meet the clinical diagnostic requirements. The study was conducted in accordance with the Declaration of Helsinki (as revised in 2013). This study was approved by the Ethics Committee of Shandong University Affiliated Children's Hospital (No. SDFE-IRB/P-2022035), and informed consent was obtained from the patients or their guardians who voluntarily signed the informed consent form.

MRI and CT imaging

MRI imaging is common clinical practice for diagnosing RB and evaluating treatment efficacy for pediatric patients. To compare the diagnostic efficacy of the two imaging modalities, a portion of the patients underwent CT scanning at the initial stage of this study.

For MRI multisequence imaging, a 3.0-Tesla superconducting magnetic resonance (MR) scanner (Ingenia, Philips, Amsterdam, the Netherlands) with a standard head coil was used. The imaging sequences included turbo spin-echo diffusion-weighted imaging (TSE-DWI), T1-weighted modified Dixon (T1W-mDIXON) contrast-enhanced scan, and T2-weighted imaging (T2WI). The TSE-DWI parameters were as follows: b-values =0 and 1,000 s/mm^2, parallel acquisition technique total scan time =1 minute and 45 seconds, echo time (TE) =51 ms, repetition time (TR) =5,365 ms, number of signals averaged (NSA) =3, field of view (FOV) =120 mm × 163 mm, matrix =80×100, slice thickness =2.0 mm, and interslice gap =0.2 mm. For the T1W-mDIXON with contrast enhanced-procedure, gadobenate dimeglumine was intravenously injected at a flow rate of 1.3 mL/s with a standard dose of 0.2 mL/kg, and four temporal scans were performed at 10-second intervals, resulting in a total scan time of 5 minutes and 50 seconds. The parameters for this sequence were as follows: TE =8.9 ms, TR =561 ms, NSA =3, FOV =120 mm × 163 mm × 39 mm, matrix =332×263, slice thickness =2.0 mm, and interslice gap =0.2 mm. For the conventional T1W-mDIXON sequences, the parameters were as follows: TE =7.1 ms, TR =638 ms, NSA =3, FOV =120 mm × 163 mm, matrix =332×263, slice thickness =2 mm, and interslice gap =0.2 mm. The T2-weighted high-resolution modified Dixon (T2W-HR-mDIXON) sequence was as follows: TE =94 ms, TR =2,500 ms, NSA =3, FOV =120 mm × 163 mm, matrix =160×105, slice thickness =2.0 mm, and interslice gap =0.2 mm. The T2WI sequence parameters were as follows: TR/TE =3,250 ms/98 ms and slice thickness =2.0 mm. Finally, the

DWI sequence parameters were as follows: number of slices =30 slices, TR =2,000 ms; TE =100 ms, slice thickness =2 mm, and FOV =500 mm × 200 mm.

CT images were obtained at the start of this study (from June 2016 to October 2016) using a multislice spiral CT (MSCT) machine (Discovery 750HD, GE HealthCare, Chicago, IL, USA) at a low-dose mode to compare the diagnostic efficacy of CT with that of MRI. To minimize radiation dose, we limited the scanning range to the upper and lower levels of the eyeball and employed an iterative reconstruction algorithm. This resulted in a significant reduction in the dose-length product (DLP) and overall dose exposure to only 0.16–0.22 mSv per scan. Prior to scanning, metal objects were removed for all patients, and sedation through enteral administration (with chloral hydrate being administered as the sedative agent at a dosage of 0.3–0.5 mg per kilogram of body weight) was required for patients who did not cooperate with CT scanning. The scanning parameters were as follows: tube voltage and current were set at 120 kV and 150 mA, respectively. The slice thickness and interval were 3 mm, and the pitch was 1.0. The scanning range extended from the upper margin of the external auditory canal to the lower margin of the orbit. To evaluate the presence of the optic nerve and intraorbital metastasis, assess the ophthalmic artery, identify vascular abnormalities and occlusions, and determine the presence of contrast enhancement within solid components, contrast-enhanced scans were conducted, with iopromide being injected after a plain scan through the antecubital vein using a high-pressure injector at a dose of 1.5–2 mL/kg.

Evaluation of differentiating RB and SOAI outcomes

Three MRI diagnostic physicians with deputy senior titles or above, each with more than 10 years of experience, reviewed the images together. They qualitatively analyzed the imaging features and quantitatively measured the pixel values in the lesion area. The accuracy of RB diagnosis using CT and MRI examinations was compared based on pathological or surgical results.

The MRI apparent diffusion coefficient (ADC) map was automatically generated with the workstation system (Philips), and all other data measurements were performed on the Lanwon Picture Archiving and Communication Systems (PACS) workstation. During the measurements, the tools were placed in the region of interest (ROI) at the maximum level of the lesion, with a distance of more than 2 mm from the edge of the lesion to avoid interference from the surrounding structures. When the diameter of the lesion was less than or equal to 3mm, the point measurement method was used. The ADC and delta signal increase (ΔSI) measurements were selected on the image at no less than three locations in the lesion area, and the average value was finally calculated. The ΔSI was calculated as the difference between pre- and post-enhancement signal intensities divided by the pre-enhancement signal intensity, multiplied by 100%. The measurement of tumor calcification volume was performed using the susceptibility-weighted imaging (SWI) sequence. The cross-sectional area of calcification was calculated for each level, which was then multiplied by the slice thickness, and the results were then summed.

Statistical analysis

SPSS 22.0 software (IBM Corp., Armonk, NY, USA) was used for statistical analysis. Continuous data are presented as the mean ± standard deviation (SD), and categorical data are represented by counts and percentages. The chi-square test for 2×2 tables, chi-square test for R × C tables, and the independent samples *t*-test were used to analyze the impact of various factors on the prognosis of pediatric patients and the differences in the success of eye preservation, failure of eye preservation, and preservation of visual acuity across different stages. Binary logistic regression was used to analyze the independent factors associated with the prognosis of pediatric patients. All results were considered statistically significant at $P<0.05$.

Results

Patients

The study included 256 patients with RB who underwent MRI examinations. Among them, successful eye preservation was achieved in 175 cases, while 81 cases failed (56 cases underwent enucleation surgery, and 25 cases resulted in death). There were 168 boys and 88 girls, with an age range of 5 to 56 months and an average age of 21.5±0.7 months. Among the patients, 83 were classified as B stage, 64 as C stage, 63 as D stage, and 46 as E stage. The main reasons for seeking medical attention were leukocoria, visual impairment, and strabismus. Among the 256 patients, 33 had both CT and MRI scans. Among these patients, 19 were male, 14 were female, and the average age was 2.11±0.26 years. Additionally, 12 patients had RB in the left eye, 19 in the right eye, and 2 had

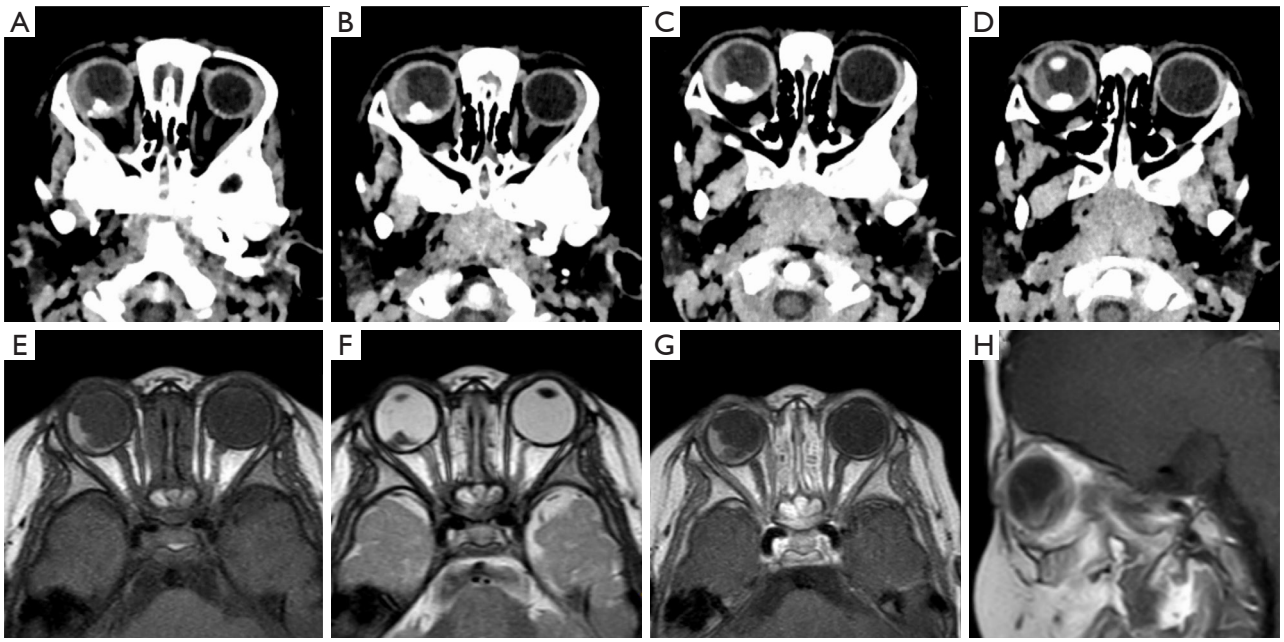

Figure 1 A 1-year and 2-month-old female patient presented with RB in the right eye. (A-D) CT axial images showed irregular nodular calcification with slightly higher density in the posterior part of the right eyeball, suggesting hemorrhage. (E-H) T1-weighted non-fat-suppressed axial plain scan, T2-weighted non-fat-suppressed axial plain scan, T1-weighted non-fat-suppressed axial enhanced scan, and T1-weighted non-fat-suppressed sagittal enhanced scan. RB, retinoblastoma; CT, computed tomography.

bilateral involvement. Clinical fundus examination revealed gray-white raised masses in the vitreous or retina, as well as neovascularization.

Evaluation of CT and MRI discrimination for RB

CT imaging findings for RB

In the CT findings of RB, a posterior intraocular mass with high-density shadow in the vitreous of the eyeball can be observed. Within the tumor, there may be spots, patches, or clustered calcifications. The CT values are mostly above 100 Hounsfield units (HU). After contrast-enhanced scanning, noncalcified tumors show varying degrees of enhancement. In this study, all 33 patients exhibited intraocular masses of soft tissue density within the eye's ciliary body, with clear boundaries. The maximum diameter of the masses was 20 mm. In 28 patients, the tumor growth was located posteriorly to the ciliary body and was accompanied by local ciliary body hyperplasia. Calcifications were observed in 30 patients, with a calcification rate of 90.90%. Among them, eight patients presented with granular or punctate microcalcifications. One patient showed a slightly high-density shadow along the inner edge of the left eyeball (*Figure 1A-1D*). Retinal detachment was observed in one case. There were no abnormal results in the posterior globe and orbit in 11 cases. One case showed overall thickening of the optic nerve with signs of enlarged optic canal and suprasellar cistern metastasis. One case had metastasis to the parotid gland.

MRI imaging findings for RB

The T1WI findings of RB include low-to-moderate signal intensity, while T2WI shows moderate-to-high signal intensity, with significant enhancement after contrast administration. In tumors with more calcifications, long T1 and short T2 signals can be observed. In the 33 patients examined in this study, the masses were mostly hypointense on T2WI and hyperintense on T1WI. One patient had bulging of the eyeball, with invasion of the lesion into the optic nerve and intraorbital structures, leading to the appearance of abnormal signals within the orbit and optic nerve thickening. In one patient, a spindle-shaped lesion with T1 shortening and T2 signals could be seen in the left eyeball (*Figure 1E-1H*). Among the enhanced scans, three patients showed obvious enhancement of the masses, whereas three patients exhibited uneven enhancement.

Table 1 Univariate analysis of the clinical features associated with the outcome of 256 children with intraocular RB

Clinical features	Eyeball retention status		χ^2/t	P
	Succeed (n=175)	Failed (n=81)		
ΔSI (%)	1.61±0.05	1.30±0.07	8.818	<0.001
ADC ($\times10^{-3}$/mm^2)	0.87±0.02	0.83±0.01	4.184	0.56
Distance between tumor and optic disc (mm)	1.69±0.15	1.20±0.24	4.229	0.002
Maximum tumor diameter (mm)	4.35±0.67	8.74±0.61	23.507	<0.001
Concomitant implant lesion	21 (12.00)	57 (70.37)	89.05	<0.001
Implant range (mm)	1.90±0.24	3.22±0.46	7.218	<0.001
Implant lesion site	n=21	n=57	7.809	0.005
Subretinal	7 (33.33)	39 (68.42)		
Vitreous cavity	14 (66.67)	18 (31.58)		
Tumor growth pattern			51.698	<0.001
Endogenous	123 (70.29)	18 (22.22)		
Ectotype	52 (29.71)	63 (77.78)		
Retinal exfoliation (mm)	2.88±0.38	6.02±0.86	11.631	<0.001
Vitreous hemorrhage	45 (25.71)	49 (60.49)	28.825	<0.001
Clinical risk factor	32 (18.29)	56 (69.14)	63.468	<0.001
Tumor calcification rate	n=148	n=77	55.728	<0.001
<20%	90 (60.81)	14 (18.18)		
20–50%	41 (27.70)	21 (27.27)		
>50%	17 (11.49)	42 (54.55)		
Atrophy of affected eyeball	37 (21.14)	54 (66.67)	50.086	<0.001

Data are presented as mean ± SD and n (%). ΔSI: difference between pre- and post-enhancement signal intensities. RB, retinoblastoma; ΔSI, delta signal increase; ADC, apparent diffusion coefficient; SD, standard deviation.

Evaluation of SOAI efficacy

First, we analyzed the treatment efficacy of SOAI and its related influencing factors. The ΔSI and the distance between the tumor and the optic disc were significantly higher in successfully treated children than in those whose treatment had failed (P=0.002). Conversely, the maximum tumor diameter, subretinal implantation rate, implantation range, exogenous tumor rate, retinal detachment range, vitreous hemorrhage rate, rate of associated high-risk factors, and rate of shrinkage in the affected eye were significantly lower in successfully treated children compared to those whose treatment had failed. There were no significant differences in tumor ADC (P=0.56), as shown in *Table 1*.

Furthermore, we evaluated the preservation rate between different stages. From *Table 2*, we can observe that the preservation rate decreased with increasing stage number, with no statistically significant difference between stages C and B (χ^2=2.577; P=0.11), while the differences between the other groups were statistically significant (P<0.001). As shown in *Table 3*, the visual acuity of successfully treated children decreased with increasing stage number, and the differences between groups were statistically significant (P<0.001).

Finally, we performed binary logistic multivariate analysis to determine the factors associated with treatment efficacy in children. The results showed that the distance between the tumor and the optic disc, clinical high-risk factors, and tumor growth pattern were independent influencing factors for treatment efficacy. Other factors

Table 2 Comparison of eye retention rate in 256 children with intraocular RB

Stages	N	Eyeball retention status		χ^2	P
		Succeed (n=175)	Failed (n=81)		
B	83	76 (91.57)	7 (8.43)	80.183	<0.001
C	64	53 (82.81)	11 (17.19)		
D	63	37 (58.73)	26 (41.27)		
E	46	9 (19.57)	37 (80.43)		

Data are presented as n (%). Comparison between stage C and B (χ^2=2.577, P=0.11). RB, retinoblastoma.

Table 3 Comparison of visual acuity of 175 children with intraocular RB after successful eye retention

Stages	Number	Vision is preserved to varying degrees (n=58)	Vision perceives only light (n=53)	Total loss of vision (n=64)	χ^2	P
B	76	38 (50.00)	31 (40.79)	7 (9.21)	48.636	<0.001
C	53	14 (26.42)	13 (24.53)	26 (49.05)		
D	37	6 (16.22)	7 (18.92)	24 (64.86)		
E	9	0 (0.00)	2 (22.22)	7 (77.78)		

Data are presented as n (%). RB, retinoblastoma.

Table 4 Multivariate logistic regression analysis of the factors predicting outcome in 256 children with RB

Clinical features	B	SE	Wald	P	OR	95% CI
ΔSI	−1.176	1.250	0.844	0.35	0.309	0.635–4.895
Maximum tumor diameter	−0.730	0.630	1.344	0.25	0.482	0.755–4.463
Distance between tumor and optic disc	1.939	0.806	5.786	0.02	6.955	1.627–28.135
Clinical risk factor	2.289	0.806	8.069	0.005	9.869	2.548–30.276
Implant lesion within eyeball	0.369	0.685	0.290	0.59	1.446	0.127–1.258
Implant lesion site	0.005	0.009	0.268	0.61	1.005	0.053–0.789
Tumor growth pattern	2.076	0.833	6.215	0.01	7.971	1.885–29.876
Retinal exfoliation	1.538	0.892	2.974	0.09	4.658	0.775–22.346
Vitreous hemorrhage	0.772	0.851	0.823	0.36	2.164	0.408–16.295
Atrophy of affected eyeball	0.946	0.849	1.243	0.27	2.576	0.488–13.593
Microcalcification	−0.338	0.828	0.167	0.68	0.713	0.141–3.612

ΔSI: difference between pre- and post-enhancement signal intensities. RB, retinoblastoma; SE, standard error; OR, odds ratio; CI, confidence interval; ΔSI, delta signal increase.

such as microcalcification were not independent factors for surgical prognosis, as shown in *Table 4*.

Discussion

This study comprised two principle parts. First, we assessed the differences in CT and MRI imaging features and evaluated their diagnostic agreement in patients with RB. Intra-arterial chemotherapy (IAC) is a chemotherapy option for intraocular RB. It involves the precise infusion of chemotherapeutic drugs into the ophthalmic artery using a catheter, leading to increased local concentrations of the

drugs within the tumor. The effectiveness of the treatment is directly related to the tumor's blood supply, as greater blood perfusion results in increased drug concentration (16). Regardless of whether it is a newly diagnosed or recurrent RB case, typically 2–4 sessions of IAC treatment are conducted. In this study, we used quantitative measurements obtained from multisequence MRI images to assess the effectiveness of SOAI treatment and evaluate the preservation rate at various stages, as well as to analyze visual acuity outcomes.

With advancements in CT techniques and imaging technology, MSCT has been widely used in clinical practice due to its advantages of fast scanning, simplicity in operation, and good repeatability. Thin-section scanning techniques effectively display calcification within RB tumors and are highly sensitive compared to MRI examinations. Manifestations of RB in MSCT include a high-density mass-like lesion in the posterior vitreous, along with various patterns of calcifications (17). CT values typically exceed 100 HU, and solid tumors exhibit enhancement to varying degrees. Prior research (18) has reported calcification rates of up to 84.9%, and in this study, the calcification rate among the 33 patients was consistent with that in the previous literature at 87.88% (29/33). Therefore, intratumoral calcification is a qualitative diagnostic criterion for RB, with higher diagnostic value occurring at younger ages. MSCT has the capability to detect small calcific foci due to its high resolution. Clinically, the presence of a tumor mass with calcification on MSCT scans in children under 3 years old may indicate RB. Notably, conditions such as Coats disease manifest as retinal detachment, subretinal fluid accumulation, absence of intraocular masses, and lack of enhancement on contrast imaging; therefore, relying solely on intratumoral calcification is insufficient for definitively diagnosing RB.

In contrast to MSCT, MRI examinations possess advantages in detecting calcification due to longer contrast agent retention time and higher sensitivity during enhancement scans (19). The enhancement pattern on MRI can also serve as a reference for prognosis evaluation, with more pronounced enhancement indicating a poorer prognosis. Typically, RB exhibits low-to-moderate signal intensity on T1WI, moderate-to-high signal intensity on T2WI, and significant enhancement after contrast administration. Tumors with extensive calcification may display T1 signal prolongation and T2 signal shortening. MRI is more sensitive to large calcific lesions but may not detect microcalcifications. However, in terms of visualizing tumor and surrounding tissue structures, MRI outperforms CT (20). In this study, when comparing CT and MRI with pathological examination as the reference, we found that the diagnostic agreement rates for RB were 96.96% and 84.84%, respectively. Both CT and MRI demonstrated high diagnostic value, with CT exhibiting slightly higher accuracy than MRI. In this study, postoperative pathological examinations of 56 enucleated patients revealed optic disc involvement, although MRI showed negative results for some patients. This suggests the presence of potential or minimal optic disc infiltration. Therefore, during the pretreatment MRI assessment, if the tumor's boundary with the optic disc is unclear or if they are in close proximity, caution should be exercised in selecting the treatment approach.

This study also analyzed the impact of various parameters on RB tumor prognosis. The results indicated that the distance between the tumor and the optic disc, clinical high-risk factors, and tumor growth pattern are closely associated with prognosis and may serve as independent influencing factors. Among successfully treated patients, the distance between the tumor and the optic disc was significantly greater than that of the cases of treatment failed. Optic disc involvement is a significant factor leading to disease progression and metastasis, as invasion of the optic nerve is the most common pathway for tumor spread outside the eyeball (21). Pathological analysis of enucleated patients in this study revealed optic disc involvement even in cases where MRI results showed negative findings, suggesting potential or mild optic disc infiltration factors. Therefore, caution should be exercised when the boundary between the tumor and the optic disc is unclear or when the distance is close, as conservative treatment may yield unsatisfactory results, necessitating early enucleation to prevent distant metastasis and protect the patient's life.

The number of failed cases accompanied by high-risk factors was significantly higher than was the number of successful cases. The use of SOAI therapy for patients with clinical high-risk factors has been a topic of debate (22,23). Some advocate for enucleation followed by adjuvant chemotherapy, while others argue against using clinical high-risk factors as a standard for enucleation. This study found that only 18.29% of successful cases were accompanied by high-risk factors, whereas 69.14% of failed cases had high-risk factors, indicating that clinical high-risk factors are prognostic risk factors. The intraocular tumor breaches the scleral wall and extends beyond the eyeball, invading the intraorbital region, making patients susceptible

to spreading during SOAI treatment and thus endangering their life. Therefore, surgical treatment is the preferred option for this subset of patients.

Tumors can grow in multiple ways, primarily through endogenous and exogenous growth patterns. Our study results indicate that endogenous tumors are more likely to achieve successful ocular preservation compared to exogenous tumors. A previous study reported no significant difference in prognosis between the two growth patterns (24), which contradicts our findings. The treatment modality may explain this disparity, as exogenous tumors grow toward the choroid, entering the orbit via the suprachoroidal space through the vortex veins, ciliary vessels, and optic nerve. This causes hemorrhagic dissemination, leading to a poorer prognosis. Conversely, endogenous tumors growing within the vitreous cavity have fewer instances of dissemination, resulting in a relatively more favorable prognosis.

Despite not being independent influencing factors, some factors are essential indicators for evaluating prognosis. The presence of tumor calcification did not significantly differ between the two groups in this study, but the volume of calcification differed significantly. The calcification range was inversely proportional to treatment efficacy, contradicting previous findings (25). Calcification reflects tumor necrosis and indicates a lack of tumor blood supply, making it difficult for chemotherapy drugs to penetrate the tumor and thus resulting in a poor prognosis.

Our study did not find a statistically significant difference in tumor ADC between the two groups. Previous research has mainly focused on using ADC to assess tumor activity after chemotherapy (26), with literature on the evaluation of tumor activity before chemotherapy being spare. RB tumors have relatively stable characteristics and a single cellular composition, making ADC unable to differentiate between different tumor cell compositions. Therefore, this indicator has limited guidance for treatment plans.

The success rate of eye preservation decreases as the tumor stage increases, contrary to previous report suggesting that for tumors in stages B to E without clinical high-risk factors, the difference in treatment outcomes after chemotherapy is not significant (27). The treatment modality and assessment criteria for tumor staging may contribute to this disparity. However, in our study, three blinded radiologists conducted evaluations according to the most recent RB intraocular staging standards and relevant MRI criteria, ensuring accurate results. The careful selection of treatments is guided by the increase in tumor stage. Stages B and C have relatively few adverse effects, with success rates above 80%, while stage E has a success rate below 20%. Once treatment fails, there is a high risk of spreading and metastasis, posing a serious threat to the child's life. Therefore, early surgical resection should be considered for children in stage E with clinical high-risk factors (28). Among the 175 successfully preserved eyes in our study, only 58 retained some degree of vision, with the majority in stages B and C. The preservation of vision is inversely proportional to the stage, indicating that early SOAI treatment can preserve visual acuity for children at lower stages of disease.

Conclusions

MRI and CT imaging have significant roles in the comprehensive assessment of tumors for pediatric RB. Due to effects of radiation dose on children, MRI alone can provide a comprehensive assessment of patients with RB. Calcification of the tumor is crucial for diagnosis, and imaging findings provide reference for patient prognosis and treatment planning. The distance between the tumor and optic disc, clinical high-risk factors, and tumor growth pattern are closely related to the prognosis of children.

Acknowledgments

Funding: This work was supported by a grant from the Jiangsu Medical Association of China (No. SYH-3201140-0087:2023034), the Suzhou Social Developing Project of China (No. SKJY2021054), and the Science and Technology Project of the Jinan Health Committee of China (No. 2022-1-46).

Footnote

Reporting Checklist: The authors have completed the STROBE reporting checklist. Available at https://tp.amegroups.com/article/view/10.21037/tp-24-2/rc

Data Sharing Statement: Available at https://tp.amegroups.com/article/view/10.21037/tp-24-2/dss

Peer Review File: Available at https://tp.amegroups.com/article/view/10.21037/tp-24-2/prf

Conflicts of Interest: All authors have completed the ICMJE uniform disclosure form (available at https://tp.amegroups.

com/article/view/10.21037/tp-24-2/coif). The authors have no conflicts of interest to declare.

Ethical Statement: The authors are accountable for all aspects of the work in ensuring that questions related to the accuracy or integrity of any part of the work are appropriately investigated and resolved. The study was conducted in accordance with the Declaration of Helsinki (as revised in 2013). This study was approved by the Ethics Committee of Shandong University Affiliated Children's Hospital (No. SDFE-IRB/P-2022035), and informed consent was obtained from the patients or their guardians who voluntarily signed the informed consent form.

References

1. Guo X, Wang L, Beeraka NM, et al. Incidence Trends, Clinicopathologic Characteristics, and Overall Survival Prediction in Retinoblastoma Children: SEER Prognostic Nomogram Analysis. Oncologist 2024;29:e275-81.
2. Abdelazeem B, Abbas KS, Shehata J, et al. Survival trends for patients with retinoblastoma between 2000 and 2018: What has changed? Cancer Med 2023;12:6318-24.
3. Norrie JL, Nityanandam A, Lai K, et al. Retinoblastoma from human stem cell-derived retinal organoids. Nat Commun 2021;12:4535.
4. Francis JH, Richards AL, Mandelker DL, et al. Molecular Changes in Retinoblastoma beyond RB1: Findings from Next-Generation Sequencing. Cancers (Basel) 2021;13:149.
5. Linn Murphree A. Intraocular retinoblastoma: the case for a new group classification. Ophthalmol Clin North Am 2005;18:41-53, viii.
6. Shields CL, Shields JA. Basic understanding of current classification and management of retinoblastoma. Curr Opin Ophthalmol 2006;17:228-34.
7. Dimaras H, Corson TW, Cobrinik D, et al. Retinoblastoma. Nat Rev Dis Primers 2015;1:15021.
8. Kaliki S, Maniar A, Patel A, et al. Clinical presentation and outcome of retinoblastoma based on age at presentation: a review of 1450 children. Int Ophthalmol 2020;40:99-107.
9. Kaewkhaw R, Rojanaporn D. Retinoblastoma: Etiology, Modeling, and Treatment. Cancers (Basel) 2020;12:2304.
10. Kletke SN, Mallipatna A, Mireskandari K, et al. Pediatric Cataract Surgery Following Treatment for Retinoblastoma: A Case Series and Systematic Review. Am J Ophthalmol 2022;239:130-41.
11. Michaels ST, Abruzzo TA, Augsburger JJ, et al. Selective Ophthalmic Artery Infusion Chemotherapy for Advanced Intraocular Retinoblastoma: CCHMC Early Experience. J Pediatr Hematol Oncol 2016;38:65-9.
12. Trinavarat A, Chiewvit P, Buaboonnam J, et al. Selective ophthalmic arterial infusion of chemotherapeutic drugs for recurrent retinoblastoma. J Pediatr Hematol Oncol 2012;34:e218-21.
13. Abruzzo T, Abraham K, Karani KB, et al. Correlation of Technical and Adjunctive Factors with Quantitative Tumor Reduction in Children Undergoing Selective Ophthalmic Artery Infusion Chemotherapy for Retinoblastoma. AJNR Am J Neuroradiol 2021;42:354-61.
14. Wyse E, Handa JT, Friedman AD, et al. A review of the literature for intra-arterial chemotherapy used to treat retinoblastoma. Pediatr Radiol 2016;46:1223-33.
15. Becker M, Stefanelli S, Rougemont AL, et al. Non-odontogenic tumors of the facial bones in children and adolescents: role of multiparametric imaging. Neuroradiology 2017;59:327-42.
16. Liu CC, Mohmood A, Hamzah N, et al. Intra-arterial chemotherapy for retinoblastoma: Our first three-and-a-half years' experience in Malaysia. PLoS One 2020;15:e0232249.
17. Cui Y, Luo R, Wang R, et al. Correlation between conventional MR imaging combined with diffusion-weighted imaging and histopathologic findings in eyes primarily enucleated for advanced retinoblastoma: a retrospective study. Eur Radiol 2018;28:620-9.
18. Levy J, Frenkel S, Baras M, et al. Calcification in retinoblastoma: histopathologic findings and statistical analysis of 302 cases. Br J Ophthalmol 2011;95:1145-50.
19. Jansen RW, de Bloeme CM, Cardoen L, et al. MRI Features for Identifying MYCN-amplified RB1 Wild-type Retinoblastoma. Radiology 2023;307:e222264.
20. Wiwatwongwana D, Kulniwatcharoen P, Mahanupab P, et al. Accuracy of Computed Tomography and Magnetic Resonance Imaging for Detection of Pathologic Risk Factors in Patients Diagnosed with Retinoblastoma. Curr

Eye Res 2021;46:1544-50.
21. Li Z, Guo J, Xu X, et al. Diagnosis of Postlaminar Optic Nerve Invasion in Retinoblastoma With MRI Features. J Magn Reson Imaging 2020;51:1045-52.
22. Zhao J, Feng Z, Leung G, et al. Retinoblastoma Survival Following Primary Enucleation by AJCC Staging. Cancers (Basel) 2021;13:6240.
23. Kaliki S, Shields CL, Cassoux N, et al. Defining High-risk Retinoblastoma: A Multicenter Global Survey. JAMA Ophthalmol 2022;140:30-6.
24. Kletke SN, Feng ZX, Hazrati LN, et al. Clinical Predictors at Diagnosis of Low-Risk Histopathology in Unilateral Advanced Retinoblastoma. Ophthalmology 2019;126:1306-14.
25. Dimaras H, Corson TW. Retinoblastoma, the visible CNS tumor: A review. J Neurosci Res 2019;97:29-44.
26. Chen S, Ji X, Liu M, et al. The value of MRI in evaluating the efficacy and complications with the treatment of intra-arterial chemotherapy for retinoblastoma. Oncotarget 2017;8:38413-25.
27. De Francesco S, Galluzzi P, Bracco S, et al. Alternated intra-arterial and intravitreal chemotherapy for advanced intraocular retinoblastoma: preliminary successful results without systemic chemotherapy. Int Ophthalmol 2015;35:887-95.
28. Rating P, Bornfeld N, Schlüter S, et al. Long-Term Results after Intraocular Surgery in Treated Retinoblastoma Eyes. Ocul Oncol Pathol 2022;8:161-7.

(English Language Editor: J. Gray)

Cite this article as: Zhao J, Cui R, Li L, Zhao B, Chen L. Multimodal imaging for the differential diagnosis and efficacy evaluation of intraocular retinoblastoma in children with selective ophthalmic artery infusion. Transl Pediatr 2024;13(7):1022-1032. doi: 10.21037/tp-24-2